Magnetic molecules as sensors of topological hysteresis of superconductors

Giulia Serrano (giulia.serrano@unifi.it)
Università di Firenze & INSTM RU https://orcid.org/0000-0001-7953-7780

Lorenzo Poggini
CNR-ICCOM

Giuseppe Cucinotta
University of Florence https://orcid.org/0000-0003-1637-0850

Andrea Sorrentino
University of Florence https://orcid.org/0000-0002-9476-4583

Niccolò Giaconi
Università di Firenze & INSTM RU

Brunetto Cortigiani
University of Florence

Danilo Longo
Synchrotron SOLEIL

Edwige Otero
Synchrotron SOLEIL

Philippe Sainctavit
Institute of Mineralogy, Materials Physics and Cosmochemistry

Andrea Caneschi
Università di Firenze https://orcid.org/0000-0001-5535-3469

Matteo Mannini (matteo.mannini@unifi.it)
Università di Firenze & INSTM RU https://orcid.org/0000-0001-7549-2124

Roberta Sessoli
University of Florence https://orcid.org/0000-0003-3783-2700

Article

Keywords:

Posted Date: January 7th, 2022

DOI: https://doi.org/10.21203/rs.3.rs-1110786/v1

Version of Record: A version of this preprint was published at Nature Communications on July 4th, 2022.
See the published version at https://doi.org/10.1038/s41467-022-31320-5.

Magnetic molecules as sensors of topological hysteresis of superconductors

Giulia Serrano,[1*] Lorenzo Poggini,[2] Giuseppe Cucinotta,[3] Andrea Luigi Sorrentino[1,3], Niccolò Giaconi,[1,3] Brunetto Cortigiani,[3] Danilo Longo,[4] Edwige Otero,[4] Philippe Sainctavit,[4,5] Andrea Caneschi,[1] Matteo Mannini,[3*] Roberta Sessoli[3]

[1] *Department of Industrial Engineering (DIEF) and INSTM Research Unit, University of Florence, Via Santa Marta 3, 50139 Florence, Italy.*
giulia.serrano@unifi.it
[2] *Institute for Chemistry of Organo-Metallic Compounds (ICCOM-CNR), Via Madonna del Piano 10, 50019 Sesto Fiorentino (FI), Italy.*
[3] *Department of Chemistry "U. Schiff" (DICUS) and INSTM Research Unit, University of Florence, Via della Lastruccia 3-13, 50019 Sesto Fiorentino (FI), Italy.*
matteo.mannini@unifi.it
[4] *Synchrotron SOLEIL, L'Orme des Merisiers, 91192 Saint-Aubin, France.*
[5] *Institut de Minéralogie, de Physique des Matériaux et de Cosmochimie (IMPMC), CNRS, Sorbonne Université, 4 place Jussieu, 75252 Paris Cedex 5, France.*

Abstract

Superconductors and magnetic materials, including molecules, are key ingredients for quantum and advanced spintronic applications. However, only a little is known about how these materials are mutually influenced at their interface in hybrid architectures. Here, we show that a single layer of magnetic molecules, the Terbium(III) bis-phthalocyaninato ($TbPc_2$) complexes, deposited on a superconducting Pb(111) surface is sensitive to the topology of the intermediate state of the superconductor, namely to the presence and evolution of superconducting and normal domains due to the magnetic field screening and penetration. The evidence of this sensitivity is found in the magnetisation dynamics of the $TbPc_2$ sub-monolayer in its paramagnetic regime showing the fingerprint of the topological hysteresis of the superconducting substrate. This study reveals the great potentialities hold by thin layers of magnetic molecules for sensing local magnetic field variation in hybrid molecular/superconductor architectures, including spin resonators or spin injection devices for spintronics applications.

Introduction

Recently, the coupling between magnetic materials and superconductors (SCs) has raised an increasing interest for its potentialities in spintronics and quantum technologies.[1,2] First, their coupling led to an enhancement of spintronic

related phenomena, such as spin injection and magnetoresistance.[1] At the nanoscale, the interaction of single spins with superconducting substrates revealed the appearance of local bound states within the SC band gap[3,4] opening a route to creating Majorana bound states which may be used as fundamental units for topological quantum computing applications.[5] Differently from individual atoms or bulk impurities, magnetic molecules profit from a well-defined chemical structure that can be engineered to tune the molecular spin coupling strength with superconducting substrates and control local bound states.[4] From a technological point of view, the realization of hybrid molecular – superconductor architectures can permit the integration of molecular qubits in quantum circuit, as superconducting microwave resonators,[6,7] or to produce dissipationless spin currents through spin singlet-to-triplet conversion mechanism.[8]

An important step forward in the research on hybrid materials comprising molecules and superconductors was achieved by some of us, depositing a single layer of single molecule magnets (SMMs) retaining their magnetic memory on Pb(111). It was shown that the transition of Pb to the superconducting state alters the magnetization dynamics of the Fe_4 SMMs complexes inducing a switching of their magnetic state from a blocked state to a resonant regime via quantum tunnelling of the magnetization.[9] This phenomenon was observed for the first time in the magnetic hysteresis loop of the SMMs layer recorded by synchrotron radiation and indicated that the superconducting transition may severely influence the magnetic properties of the molecular film at a large scale. Besides these seminal results, a deep understanding of the key ingredients characterizing the interface between molecules and superconductors was necessary to explore the frontiers of the molecular sensitivity to the superconducting state. For this reason, here we growth on top of a Pb(111) single crystal a layer of a more anisotropic SMM, the Terbium(III) bis-phthalocyaninato ($TbPc_2$) complex, that is known to significantly interact with the metallic surfaces.[10–12] $TbPc_2$ is a double-decker system formed by two phthalocyanines (Pc) coordinating a Tb^{III} ion[13–17] (**Figure 1a**). The complex is characterized by a strong uniaxial anisotropy with the easy axis of the magnetization oriented perpendicularly to the Pc planes (**Figure 1a**). Near liquid helium temperatures and in bulk crystals, it behaves as a single molecule magnet thanks to the large energy barrier separating the ground doublet states ($J_z = \pm 6$) that hinders the reversal of the magnetization. At variance with Fe_4 SMM complexes,[18,19] both the electronic and magnetic properties of $TbPc_2$ are particularly sensitive to the interaction with substrates. The signature of this interaction was observed on a wide range of metallic and non-metallic substrates either at the single molecule level or at the larger scale of the molecular film.[20–22] Remarkable effects were found in the magnetic hysteresis loop of $TbPc_2$ films, which is quenched for molecules directly interacting with metals while preserved or improved by the use of decoupling layers[21–23] or anchoring groups.[24] Small apertures of the hysteresis loop were found only for $TbPc_2$ monolayer on TiO_2 films,[25] graphene[21] or HOPG[26] substrates. On the other side, MgO films separating the $TbPc_2$ from the metal Ag(100) surface, led to large magnetic remanence and the disappearance of the quantum tunnelling of the magnetisation at zero field.[22]

The sensitivity of $TbPc_2$ films to the environment has been here exploited to investigate the magnetization of $TbPc_2$ at the interface with Pb(111) and across its superconducting transition, as a function of the temperature and magnetic field. To achieve this purpose, we deposited by thermal sublimation a sub-monolayer of $TbPc_2$ molecules directly on Pb(111). The study, performed by *in house* surface characterization methods (*e.g.* Scanning Tunnelling Microscopy, STM, and X-ray Photoelectron Spectroscopy, XPS) and synchrotron radiation, showed that the magnetization curve of the investigated $TbPc_2$ sub-monolayer is influenced by the topology of the superconducting and normal domains of Pb when the magnetic field intensity is raised or lowered. This effect causes the opening of the hysteresis loop of $TbPc_2$ within the superconducting regime of the substrate, which is ascribed to the topological hysteretic behaviour of the substrate.

Results

The Pb(111) crystal was prepared according to the procedure reported in the Methods and preliminarily characterized by XPS and STM (see **Figure S1**). The molecular deposit on Pb(111) was obtained by thermal sublimation of the $TbPc_2$ powder dosing a sub-monolayer amount (see Methods). The growth and adsorption configuration of $TbPc_2$ on Pb(111) was studied by STM at low temperature (35 K) and low surface coverage (~ 30%). **Figure 1b** shows a 3D STM image of the $TbPc_2$ sub-monolayer on Pb(111). The image shows large Pb(111) terraces with monoatomic steps (indicated by yellow arrows) of about 0.3 nm height.[9] The black arrow indicates an island of $TbPc_2$ molecules deposited on the clean Pb(111) surface. The formation of regular islands is common for the deposition of $TbPc_2$ thin films on many other surfaces.[22,27,28] The height of the island is about 0.5 nm, consistently with the distance between the two Pc planes. This also indicates that the molecules maintain the lying down configuration (Pc planes parallel to the surface), mostly observed on metal surfaces.[21,22,27,28] The $TbPc_2$ sub-monolayer on Pb(111) was characterized by XPS at room temperature to study the molecular stoichiometry and interaction with the substrate (see Methods) evidencing spectral features (**Figures 1c and d and Figure S2**) in line with those observed for monolayer or thick films on other surfaces.[29–31] The C*1s* spectrum of the $TbPc_2$ film on Pb is characterized by two main components at 284.5 eV and 285.4 eV ascribed to C-C and C-N bonds, and related shake-up signals at 286.4 eV and 288.0 eV.[29,30] The N*1s* spectrum shows the main component at 398.5 eV and a shake-up at 400.4 eV. [29–31] In **Figure S2** are also reported the XPS Pb*4f* spectrum after molecular deposition, showing the Pb$4f_{7/2}$ calibrated at 136.9 eV, and the Tb*3d* region, showing the $3d_{3/2}$ signal at 1276 eV.[9,30,32,33] We remark that the Tb$3d_{5/2}$ signal overlaps with the Auger lines of Pb and C, α-$N_6O_{4,5}O_{4,5}$ and KVV,[34] respectively, and it cannot be used for quantitative analysis. However, the C/N XPS signal ratio is 3.8, in close agreement with that expected from the molecular stoichiometry ($C/N_{theory} = 4$) and indicates the integrity of the molecular layer.

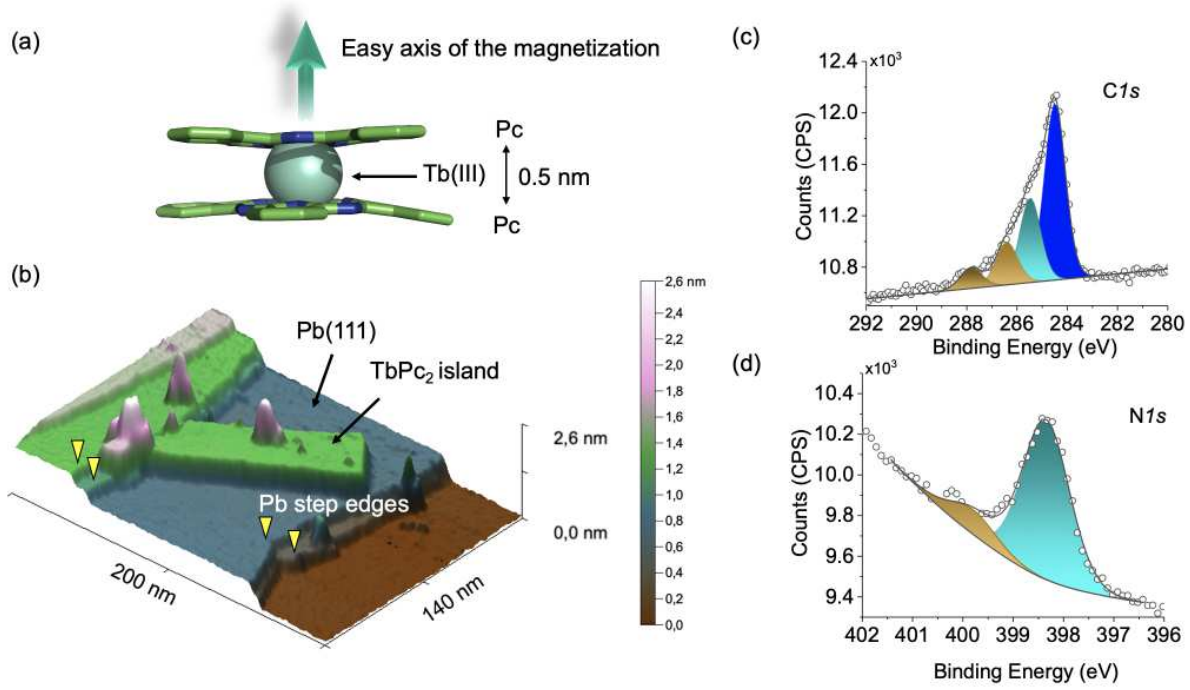

Figure 1. Structural characterization of the $TbPc_2$ sub-monolayer on Pb(111). (a) Scheme of the $TbPc_2$ structure. Colour code: green, carbon; blue, nitrogen; light cyan, terbium, hydrogens are omitted for clarity. The easy axis of the magnetisation is directed perpendicularly to the phthalocyanine (Pc) planes and sketched by an arrow. (b) 3D STM image of a $TbPc_2$ island on Pb(111) recorded at 35K (I_{tunnel}= 5 pA, V_{bias}= 2 V). The Z-colour scale is shown on the right. (c) C*1s* and (d) N*1s* XPS core-level spectra of the $TbPc_2$ sub-monolayer on Pb(111). Main components are shown in blue and cyan; shake-up components are shown in brown.

Synchrotron characterization was performed to investigate the magnetic properties of the $TbPc_2$ sub-monolayer on Pb(111) by X-ray Absorption Spectroscopy (XAS), see **Figure 2a-c**. All the measurements were recorded in the Total Electron Yield (TEY) mode (see Methods) with the magnetic field and X-ray beam axis at an angle θ from the sample's surface normal (see inset **Figure 2b**). XAS spectra were recorded using the positive (σ^+) and negative (σ^-) circular polarisation of the X-ray light to obtain the X-ray Magnetic Circular Dichroism (XMCD) spectrum ($\sigma^- - \sigma^+$) at the Tb $M_{4,5}$ edges. **Figure 2a** shows the XAS and XMCD spectra recorded at normal incidence (θ = 0°), 2 K and 3 T. The XMCD intensity value is normalised respect to the edge jump value of the isotropic XAS spectrum (see Methods). The strong dichroic signal at the M_5 edge, 1237 eV, has an intensity of about 140%, in good agreement with $TbPc_2$ monolayer and thick films previously investigated.[20–24] Indeed, this XMCD spectrum is representative of saturated Tb^{III} ions with total angular momentum J = L + S = 6 and in the symmetry imposed by the two Pc ligands.[20,35] At θ = 45°, the intensity of the XMCD signal slightly decreases to about 120% (see **Figure S3 (a)**) as a consequence of the uniaxial anisotropy of $TbPc_2$ molecules that are oriented with their easy axis of magnetisation perpendicular to the surface.[20] In **Figure S3(b)** and **(c)** are also reported the XMCD spectra recorded for θ = 0° and 3T at 4K and 8 K, respectively, which show the preservation of the strong dichroic signal at 1237 eV of the M_5 edge, as expected for a sub-monolayer coverage.[20–24]

At θ = 45°, XAS spectra were also recorded using linear vertical (σ^V) and horizontal (σ^H) light polarisation, whose difference ($\sigma^V - \sigma^H$) provides the X-ray Natural Linear Dichroism (XNLD) spectrum. The XNLD contribution

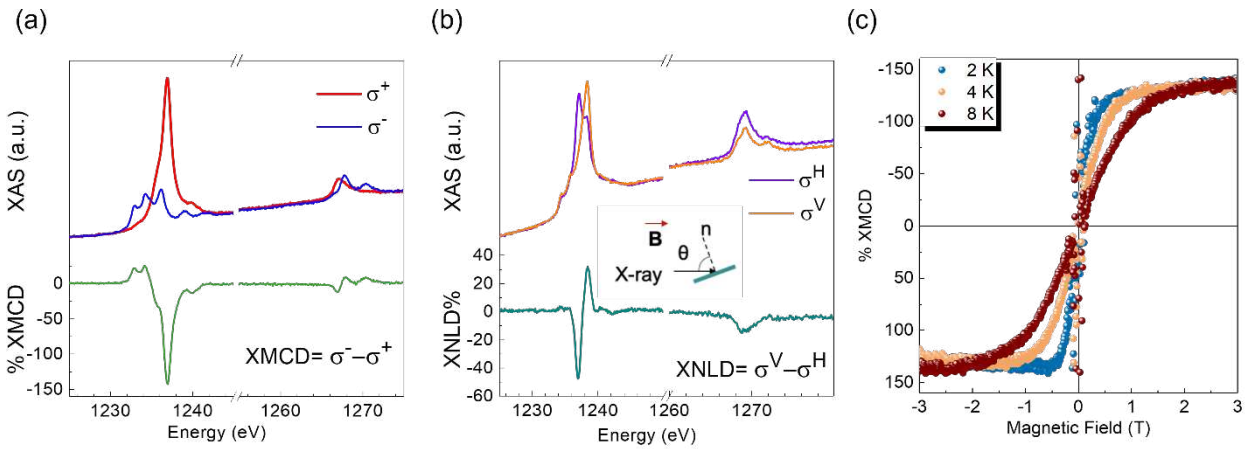

Figure 2. Magnetic characterisation of the $TbPc_2$ monolayer on Pb(111). (a) XAS and XMCD spectra recorded at θ = 0°, 2 K and 3 T. (b) XAS and XNLD spectra recorded at θ = 45°, 2 K and 3 T. (c) Magnetic hysteresis loop recorded at θ = 0° and at different temperatures (2 K, blue; 4 K, orange; 8 K, red).

gives information about the alignment of molecules in the layer and it can be used to determine the orientation of $TbPc_2$ molecules on the surface.[20,21] The XNLD spectrum for the $TbPc_2$ sub-monolayer on Pb(111), expressed in percentage according to the formula reported in the Methods, is shown in **Figure 2b**. The shape of the dichroic signal, presenting a minimum at 1237 eV with an intensity of about -50%, is a confirmation of the lying down orientation of the molecules in the monolayer, and a narrow distribution of the orientation similarly to highly oriented $TbPc_2$ films on graphene and gold substrares.[20,21]

Magnetic field dependence of the XMCD signal at the Tb M_5 edge, 1237 eV, and before the pre-edge value, 1225eV, was measured to extract the trend of the normalized XMCD while sweeping the magnetic field (see Methods) and follow the magnetic behaviour of the absorber. **Figure 2c** shows the trend obtained scanning magnetic field directed perpendicular to the sample surface (θ = 0°) with a scan rate of 0.02 T/s from -3T to 3T and vice versa. The figure shows the temperature dependence of these loops at 8 K, 4 K and 2 K (the error on the temperature value is estimated to be less than 10% of the value). As expected, given the magnetic anisotropy of the investigated sample, by decreasing the temperature increases the steepness of the curves at low fields, and decreases the field at which saturation is reached. At 2 K, the dichroism at saturation is about 140%, coherently with the intensity of the maximum dichroic signal in the XMCD spectrum recorded at 3 T and shown in **Figure 2a**. At all temperatures, the expected opening due to the SMM behaviour is quenched, and $TbPc_2$ molecules act as paramagnets. This behaviour is typical of monolayers of $TbPc_2$ deposited on metals.[12,20,22,23,36] On the other hand, the interest in this magnetic molecule/superconductor hybrid resides in the sensitivity given by the strong uniaxial magnetic anisotropy of the $TbPc_2$ complex to the superconducting transition.

The Pb(111) substrate is superconductive below its critical temperature, $T_C = 7.2\ K$, and within the critical field value H_C that varies with the temperature according to the formula $H_C(T) = H_C(0)[1 - \left(\frac{T}{T_C}\right)^2]$ (1).[37] Being $H_C(0) = 0.08\ T$ for Pb,[38] H_C is expected to be at 0.074 T at 2 K. Thus, is in the previous measurements

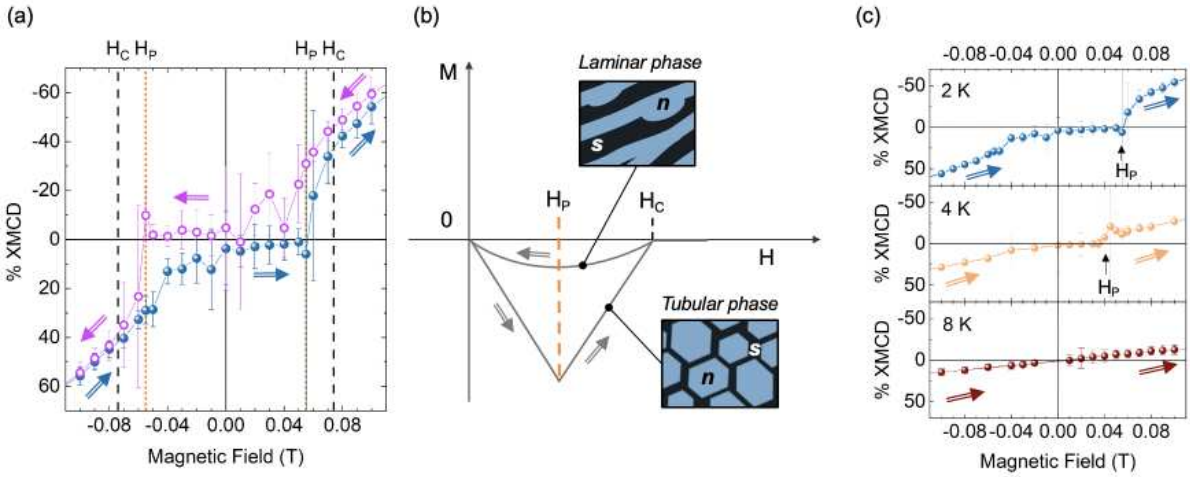

Figure 3. Magnetic behaviour of the $TbPc_2$ sub-monolayer on Pb(111) across the superconducting transition. (a) Magnetisation curves of $TbPc_2$ monolayer on Pb(111) at 2K and θ = 0° within the critical field of the superconductor (H_C). The complete magnetic field screening effect of Pb is observed for increasing magnetic field intensity within a certain field H_P. Symbol code: up branch, filled circles; down branch, empty circles; arrows indicate the field scan direction. (b) Sketch of a typical magnetisation loop of disk shaped Pb single crystals (see Ref. [41]). The hysteresis loop of bulk Pb crystals originates from the different topology of the intermediate state when the magnetic flux penetrates or is expelled from the substrate. The topology (tubular and laminar) of the micrometric superconducting (***s***) and normal (***n***) domains in the intermediate state depicted in the figure is representative of the magnetooptical images of Pb crystals of Ref. [41]. (c) Magnetization curve (up branch) of $TbPc_2$ on Pb(111) for θ = 0° at different temperatures below (2 K and 4 K) and above (8 K) the critical temperature.

(**Figure 2c**) the magnetic field region within H_C is hidden below the limit of the scan resolution adopted and below the strong noise of the XMCD signal detected by the TEY when the field is swept across zero.

To overcome this limitation, instead of acquiring the TEY signal during a magnetic field sweep, magnetisation curves were collected for each X-ray light polarization by integrating over time the TEY signal at each sampled field (see Methods). **Figure 3a** shows that at 2K, the trend of the $TbPc_2$ XMCD signal within the superconducting regime of Pb, is strongly influenced, presenting an hysteretic behaviour. We observe that by decreasing the magnetic field intensity below the Pb critical field ($|H_C| = 0.072$ T), the XMCD values of $TbPc_2$ follows an almost linear trend. In this region the effect of the superconducting transition in the $TbPc_2$ magnetization curve is therefore negligible, indicating that the magnetic field is only partially screened by the superconductor. However, after crossing zero field and increasing the magnetic field intensity, the XMCD values are zero (within the error limits) until a certain field $|H_P| = 0.055$ T. This suggest that, on the contrary, in this regime the magnetic field is completely screened out by the Pb substrate. By increasing the field above H_P, the XMCD values suddenly increase, as the superconductor is back in a regime where only partial magnetic field screening occurs before it turns into the normal state at H_C.

The fact that the $TbPc_2$ XMCD trend of **Figure 3a** shows a hysteretic behaviour is the signature of the transition of the Pb(111) crystal to the superconducting state and – in particular – of different topology of the normal (***n***) and superconducting (***s***) domains when the magnetic flux is penetrating or exiting the superconductor. It is well-established that type I superconductors below their critical field, H_C, and critical temperature, T_C, are characterized by an intermediate

state (IS) in which both ***s*** (where the magnetic field is completely expelled) and ***n*** domains (where the magnetic field penetrates) coexist at the micrometric scale. [37,39–43] The topology, *i.e.* the shape of these domains, strongly differs during the increase (magnetic flux penetration phase) or decrease (magnetic flux expulsion phase) of the magnetic field intensity. This effect was observed by magneto-optical (MO) images for various type I SCs metals,[39,44] including Pb crystals.[37,40,41] The combination of MO and SQUID measurements demonstrated that the topological variation of the IS domains causes a hysteretic behaviour (topological hysteresis).[37,40,41] In particular, Prozorov[41] treated the case of disk-shaped Pb crystals (of shape and dimensions comparable with the Pb substrate used here) in an axial magnetic field (i.e., along the cylinder axis).

A clear interpretation of the $TbPc_2$ hysteresis at 2.0 K shown in **Figure 3a** can be indeed achieved by comparing the magnetization curves of $TbPc_2$ film in light of the magnetization curves of Pb crystals reported by Prozorov[41] and here sketched in **Figure 3b**. We remark that the X-ray beam used for the measurements of **Figure 3a** has a spot diameter of about 800 μm that averages over ***s*** and ***n*** domains of micrometric size and that it is positioned at the centre of the crystal during the measurements. Following the curve sketched in **Figure 3b**, by decreasing the field below H_C, *i.e.* during the magnetic flux expulsion, the magnetisation curve of the Pb crystal shows small magnetisation absolute values, poorly affecting the magnetisation of $TbPc_2$ whose trend is only slightly deviated from linearity below H_C (see **Figure 3a**). According to Prozorov,[41] in these conditions the ***s*** and ***n*** domains of the Pb crystal show a *laminar topology* (see the sketch in **Figure 3b**). The magnetic flux can exit the sample only through the ***n*** domains which shrink on lowering the magnetic field intensity until reaching zero field, where the substrate is completely superconducting, and the magnetic flux is completely excluded (Meissner state). It is worth noticing that when the intermediate state has a laminar topology, the magnetic flux is never fully screened by the superconductor until the external magnetic field is zero. By increasing the magnetic field intensity from zero, the magnetic field does not penetrate the bulk of the sample which remains in an almost diamagnetic state until H_P (negative linear slope in **Figure 3b**).[41,45] In these conditions magnetic flux can only enter at the edges of the Pb disks but cannot migrate towards its centre,[41,45] which justifies the overall zero XMCD values detected on the $TbPc_2$ layer when the field is increased from zero to $|H_P| = 0.055$ T. When magnetic field is increased above H_P, magnetic field penetrates through ***n*** domains that expand from the sample edges over whole substrate with a *tubular topology*, where an hexagonal symmetry is favoured (see the sketch in **Figure 3b**).[41] In this phase, $TbPc_2$ molecules acting as sensors feel an increasing XMCD signal due to the expansion of the ***n*** domains **(Figure 3a)**. We remark that in the intermediate state the magnetic field intensity in normal regions is always equal to H_C[37,45] and that the increasing of the XMCD intensity here detected is only due to the average over ***n*** domains of increasing extension. Furthermore, we notice that the XMCD error bar amplitude is maximum at the onset of field penetration in tubular topology; this effect is not observed at the entrance of the SC state (field exclusion onset), where $TbPc_2$ is already

magnetized. The same behaviour was found in the hysteresis curve of Fe_4 complexes on Pb,[9] and it could be ascribed to the abrupt change in the local magnetic induction of the $TbPc_2$ molecules (and of the photoelectrons and secondary electrons of the TEY signal) when exiting the demagnetized condition.[9]

The hysteretic behaviour of the $TbPc_2$ XMCD signal shown in **Figure 3a** is maximum at H_P, and the XMCD values are null at zero field, compatibly with the topological hysteresis curves of the SC and further indicating that the hysteresis loop is not a consequence of flux pinning inside the superconductor.[41] We remark that the topological hysteretic behaviour of Pb could not have been previously observed with Fe_4 complexes, due to their SMM properties.[9] The strong drop of the Fe_4 magnetization value observed during magnetic field screening, *i.e.* lowering the magnetic field intensity below Hc, was a consequence of the average decrease of the magnetic field intensity felt by the molecules that performed the quantum tunnelling of the magnetization on ***s*** regions of increasing width. On the contrary, Fe_4 molecules could not be sensitive to the onset of field penetration (and exit from the superconducting state) since in this field range they could not be magnetized until the first field-induced level crossing was reached.[9] The paramagnetic character of $TbPc_2$ allows an enhanced sensitivity to the magnetic flux variation on the surface of the superconductor also in this field region.

A closer look to the magnetisation curve of **Figure 3a**, further support our interpretation. Indeed, the onset of the field penetration inside the superconductor varies with the geometry of the superconducting sample, which determines its demagnetizing factor (N). Being $H_P = (1 - N)H_C$[37,41] (2) and considering the experimental H_P value observed in the hysteresis loop at 2 K, we derive an N value for our Pb crystal of about 0.25. This value compares well with that extracted by Prozorov (N=0.55),[41] taking into accounts the different thickness-to-width ratio of the two substrates.[46]

Figure 3c compares the magnetisation curve of $TbPc_2$ on Pb(111) - up branch - recorded at 2 K, 4 K and 8 K. The curves show for negative fields the magnetic field expelled from the superconductor and at positive fields, the magnetic field entry. It is evident that the H_P field, *i.e.* the onset of the field penetration, changes with the temperature (at 4 K and 2 K) while it cannot be identified at 8 K. According to equation (1) and (2), at 4.2 K, H_C is expected at 0.053 T, and H_P at 0.04 T assuming N = 0.25. The XMCD data at 4 K perfectly support this hypothesis. Finally, the magnetisation curve at 8 K does not evidence the signature of the superconducting transition since it is recorded above the T_C value. The latter evidence, further demonstrate the sensitivity of a single layer of $TbPc_2$ molecules to the superconducting transition.

Conclusions

In conclusion, we deposited a single layer of $TbPc_2$ molecules by thermal sublimation in ultra-high vacuum on a clean Pb(111) surface and we characterized their interface properties by XPS and STM to check the molecular film growth and stoichiometry. Synchrotron light was used to address the magnetic behaviour and the molecular ordering of

the $TbPc_2$ film on a on a millimeter range by XMCD and XNLD, respectively. X-ray detected magnetisation measurements performed at the Tb edge showed that the $TbPc_2$ monolayer behaves as a paramagnet when the substrate is in the normal state, as typically observed for monolayer deposits on metal surfaces. However, an opening of the hysteresis loop was observed below the transition of Pb to the superconducting state. We ascribe this phenomenon to the topological hysteresis loop of the superconducting Pb(111) surface, due to the different shape of superconducting and normal domains during magnetic field penetration or expulsion. Further, from the analysis of the superconductor hysteresis loop probed by the molecules and its temperature dependence we derived the critical field and the geometrical factors of the Pb crystal that characterized the transition to the condensate state.

At variance with Fe_4 SMMs complexes,[9] we showed here that a single layer of magnetic molecules can be sensitive not only to the transition to the superconducting state but also to the topological features of superconducting domains. We stress that such sensitivity was achieved on a single layer of $TbPc_2$ in its paramagnetic regime in direct contact with the Pb substrate, which opens the perspective of using the plethora of molecules with spin properties (including highly coherent systems[47,48]) for detecting superconductivity on a large scale. Thus, $TbPc_2$ is a peculiar probe thanks to the strong magnetic anisotropy and out-of-plane magnetic susceptivity and to the capabilities to form highly oriented films that make them extremely sensitive to local magnetic flux variation.

Looking this observation form another point of view, we also demonstrated that the intrinsic topology of the intermediate state of the superconductor can induce a hysteretic behaviour in an ensemble of paramagnetic molecules. This last outcome might have a great potential for technological applications. Furthermore, these results are significant also for those fields that exploit hybrid molecular/superconductor systems in macroscopic devices, as resonators,[6,7] or for the detection of localised states occurring at the interface between single spins and superconducting surfaces,[4] where magnetic field screening effects can play an important role.

Methods

The Pb(111) single crystal was acquired from the Surface Preparation Laboratory (SPL) and it had a disk shape with a diameter of 4 mm and a height of 2 mm. The surface was prepared in ultra-high vacuum (UHV) by sputtering cycles of Ar^+ at 1500 eV and annealing at 473 K for 30 min. Before molecular deposition, surface cleanliness was checked by XPS and STM measurements at room temperature (RT). The molecular deposition was performed by thermal sublimation of the molecular powders using a homemade effusion cell. The sublimation temperature of $TbPc_2$ was 710 K and the flux was estimated by a quartz microbalance. Surface coverage was checked by STM using an Omicron VT-STM with a W tip. STM measurements were carried out by cooling down the sample to 35 K with a helium flux to reduce molecular mobility on the surface.

XPS measurements were carried out using a monochromatic Al Kα radiation (hν = 1486.6 eV, SPECS mod. XR-MS focus 600) and a SPECS Phoibos 150 1DLD electron analyser mounted at 54.44° with respect to the X-ray beam. XPS measurements were performed at normal emission with the pass energy set to 40 eV. Spectra were analysed using the CasaXPS software and calibrated at the Pb$4f_{7/2}$ signal at 136.9 eV (see Figure S2, ESI). Spectra were fitted with a linear or tougard background[49] and single-peak components were deconvoluted using a mixed Gaussian and Lorentzian function (70/30). All the above-mentioned *in house* characterizations were performed on the very same sample without breaking the vacuum.

X-ray absorption spectroscopy (XAS) experiments were carried out at the DEIMOS beamline, synchrotron SOLEIL (Saint-Aubin, France).[50] All samples were prepared and characterized in Florence and transferred to the end-station using a UHV suitcase ($P_{base} = 5 \cdot 10^{-10}$ mbar). XAS spectra were recorded in total electron yield (TEY) mode[51] using both linear and circularly polarized light[51] in a temperature range between 8.0 ± 0.2 and 2.0 ± 0.1 K and magnetic field within ± 3T (measurements' parameters are specified in the text). XAS spectra were recorded at the Tb $M_{4,5}$ edges at angles θ, defined as the angle between the ***k*** X-ray propagation vector and the surface normal. XMCD spectra were normalized to the M_5 edge jump of $(\sigma^+ + \sigma^-)/2$ and expressed in percentage (% XMCD), while XNLD spectra at θ=45° were normalized to the M_5 edge jump of the isotropic spectrum ($\sigma^{iso} = 1/3\sigma^V + 2/3\sigma^H$) and expressed in percentage (% XNLD).[52] XAS and dichroic spectra were calibrated by setting the maximum of the XMCD and XNLD at the Tb M_5 edge to 1237 eV. Magnetic hysteresis curves were obtained by recording the field dependence of the % XMCD at the Tb M_5 edge (measured at 1237 eV and here referred to the pre-edge dichroism at 1225 eV) sweeping the magnetic field between -3 T and 3 T with a scan rate of 2 T/s. Data treatment for XMCD, XNLD and hysteresis was performed employing the program pyDichroX.[53] To avoid the noise present in the TEY signal during the field sweeping when the magnetic field is close to zero, the magnetic hysteresis at low field intensities (**Figure 3**) were acquired by recording the TEY signal at each sampled field and for each X-ray light polarization (circular left and right) using a time-scan acquisition (scan time 120 s with 0.2 s of integration time for a total of 600 data points). This procedure was adopted for both the edge and pre-edge energies to get the normalised dichroic signal. The XMCD values and the associated error bars reported in the hysteresis of **Figure 3** were then obtained considering the average of TEY signal at each field, polarization and energy and the relative standard deviation.

Acknowledgements

We thank for the financial support the European COST Action CA15128 MOLSPIN and the FET Open FATMOLS project, Italian MIUR for "Progetto Dipartimenti" di Eccellenza 2018-2022 (ref. no. B96C1700020008), Regione Toscana POR CreO FESR 2014-2020- SENSOR, and Fondazione Cassa di Risparmio di Firenze (Project SPINE-2 2020.1634).

We acknowledge SOLEIL for the provision of the synchrotron radiation facilities. We thank P. Ohresser and L. Joly for assistance in using the DEIMOS beamline (project 20201244).

Author contributions

G.S., L.P., A.L.S., and B.C. prepared the sample and performed in house characterization. G.S., L.P. A.L.S., G.C., N.G., D.L., M.M., P.S. and E.O. performed synchrotron experiments. G.S., L.P., and G.C. performed and discussed the experiments. G.S. drafted the manuscript. A.C., R.S. P.S. and M.M. supervised the work. All authors have contributed and approved the final version of the manuscript.

References

1. Linder, J. & Robinson, J. W. A. Superconducting spintronics. *Nat. Phys.* **11**, 307–315 (2015).
2. Han, W., Maekawa, S. & Xie, X.-C. Spin current as a probe of quantum materials. *Nat. Mater.* **19**, 139–152 (2020).
3. Franke, K. J., Schulze, G. & Pascual, J. I. Competition of Superconducting Phenomena and Kondo Screening at the Nanoscale. *Science* **332**, 940–944 (2011).
4. Malavolti, L. *et al.* Tunable Spin-Superconductor Coupling of Spin ½ Vanadyl-Phthalocyanine Molecules. *Nano Lett.* **18**, 7955–7961 (2018).
5. Nadj-Perge, S. *et al.* Observation of Majorana fermions in ferromagnetic atomic chains on a superconductor. *Science* **346**, 602–607 (2014).
6. Bonizzoni, C. *et al.* Coherent coupling between Vanadyl Phthalocyanine spin ensemble and microwave photons: towards integration of molecular spin qubits into quantum circuits. *Sci. Rep.* **7**, 13096 (2017).
7. Gimeno, I. *et al.* Enhanced Molecular Spin-Photon Coupling at Superconducting Nanoconstrictions. *ACS Nano* **14**, 8707–8715 (2020).
8. Rogers, M. *et al.* Spin-singlet to triplet Cooper pair converter interface. *Commun. Phys.* **4**, 69 (2021).
9. Serrano, G. *et al.* Quantum dynamics of a single molecule magnet on superconducting Pb(111). *Nat. Mater.* **19**, 546–551 (2020).
10. Schwöbel, J. *et al.* Real-space observation of spin-split molecular orbitals of adsorbed single-molecule magnets. *Nat. Commun.* **3**, 953 (2012).
11. Vitali, L. *et al.* Electronic Structure of Surface-supported Bis(phthalocyaninato) terbium(III) Single Molecular Magnets. *Nano Lett.* **8**, 3364–3368 (2008).
12. Stepanow, S. *et al.* Spin and orbital magnetic moment anisotropies of monodispersed

bis(Phthalocyaninato)terbium on a copper surface. *J. Am. Chem. Soc.* **132**, 11900–11901 (2010).

13. Urdampilleta, M., Klyatskaya, S., Cleuziou, J.-P., Ruben, M. & Wernsdorfer, W. Supramolecular spin valves. *Nat. Mater.* **10**, 502–6 (2011).

14. Thiele, S. *et al.* Electrical Readout of Individual Nuclear Spin Trajectories in a Single-Molecule Magnet Spin Transistor. *Phys. Rev. Lett.* **111**, 037203 (2013).

15. Vincent, R., Klyatskaya, S., Ruben, M., Wernsdorfer, W. & Balestro, F. Electronic read-out of a single nuclear spin using a molecular spin transistor. *Nature* **488**, 357–360 (2012).

16. Bogani, L. & Wernsdorfer, W. Molecular spintronics using single-molecule magnets. *Nat. Mater.* **7**, 179–186 (2008).

17. Urdampilleta, M., Klayatskaya, S., Ruben, M. & Wernsdorfer, W. Magnetic interaction between a radical spin and a single-molecule magnet in a molecular spin-valve. *ACS Nano* **9**, 4458–4464 (2015).

18. Malavolti, L. *et al.* Magnetic Bistability in a Submonolayer of Sublimated Fe_4 Single-Molecule Magnets. *Nano Lett.* **15**, 535–541 (2015).

19. Mannini, M. *et al.* Magnetic memory of a single-molecule quantum magnet wired to a gold surface. *Nat. Mater.* **8**, 194–197 (2009).

20. Margheriti, L. *et al.* X-Ray Detected Magnetic Hysteresis of Thermally Evaporated Terbium Double-Decker Oriented Films. *Adv. Mater.* **22**, 5488–5493 (2010).

21. Serrano, G. *et al.* Magnetic bistability of a $TbPc_2$ submonolayer on a graphene/SiC(0001) conductive electrode. *Nanoscale* **10**, 2715–2720 (2018).

22. Wäckerlin, C. *et al.* Giant Hysteresis of Single-Molecule Magnets Adsorbed on a Nonmagnetic Insulator. *Adv. Mater.* **28**, 5195–5199 (2016).

23. Malavolti, L. *et al.* Magnetism of $TbPc_2$ SMMs on ferromagnetic electrodes used in organic spintronics. *Chem. Commun.* **49**, 11506–11508 (2013).

24. Mannini, M. *et al.* Magnetic behaviour of $TbPc_2$ single-molecule magnets chemically grafted on silicon surface. *Nat. Commun.* **5**, 4582 (2014).

25. Sorrentino, A. L. *et al.* A $TbPc_2$ sub-monolayer deposit on Titanium Dioxide ultrathin film: a magnetic, morphological, and chemical insight. *J. Mater. Chem. C* **9**, 15011–15017 (2021).

26. Gonidec, M. *et al.* Surface Supramolecular Organization of a Terbium(III) Double-Decker Complex on Graphite and its Single Molecule Magnet Behavior. *J. Am. Chem. Soc.* **133**, 6603–6612 (2011).

27. Serrano, G. *et al.* Bilayer of Terbium Double-Decker Single-Molecule Magnets. *J. Phys. Chem. C* **120**, 13581–13586 (2016).

28. Komeda, T., Isshiki, H., Liu, J., Katoh, K. & Yamashita, M. Variation of Kondo Temperature Induced by Molecule–Substrate Decoupling in Film Formation of Bis(phthalocyaninato)terbium(III) Molecules on Au(111). *ACS Nano* **8**, 4866–4875 (2014).

29. Serrano, G. *et al.* Substrate mediated interaction of terbium(III) double-deckers with the TiO_2 (110) surface. *Phys. Chem. Chem. Phys.* **23**, 12060–12067 (2021).

30. Cucinotta, G. *et al.* Tuning of a Vertical Spin Valve with a Monolayer of Single Molecule Magnets. *Adv. Funct. Mater.* **27**, 1703600 (2017).

31. Diller, K. *et al.* Magnetic properties of on-surface synthesized single-ion molecular magnets. *RSC Adv.* **9**, 34421–34429 (2019).

32. Bozack, M. J. & Bryant, K. W. Elemental Lead by XPS. *Surf. Sci. Spectra* **1**, 324–327 (1992).

33. Pedrini, A. *et al.* Self-Assembly of $TbPc_2$ Single-Molecule Magnets on Surface through Multiple Hydrogen Bonding. *Small* **14**, 1–7 (2017).

34. Powell, C. J. Recommended Auger parameters for 42 elemental solids. *J. Electron Spectros. Relat. Phenomena* **185**, 1–3 (2012).

35. Pineda, E. M., Komeda, T., Katoh, K., Yamashita, M. & Ruben, M. Surface confinement of $TbPc_2$-SMMs: structural, electronic and magnetic properties. *Dalt. Trans.* **45**, 18417–18433 (2016).

36. Studniarek, M. *et al.* Understanding the Superior Stability of Single-Molecule Magnets on an Oxide Film. *Adv. Sci.* **6**, 1901736 (2019).

37. Poole, C. P., Farach, H. A., Creswick, R. J. & Prozorov, R. *Superconductivity*. (Elsevier Science, 2014).

38. Chanin, G. & Torre, J. P. Critical-Field Curve of Superconducting Lead. *Phys. Rev. B* **5**, 4357–4364 (1972).

39. Huebener, R. P. *Magnetic Flux Structures in Superconductors : Extended Reprint of a Classic Text*. (Springer Berlin Heidelberg, 2001).

40. Prozorov, R., Giannetta, R. W., Polyanskii, A. A. & Perkins, G. K. Topological hysteresis in the intermediate state of type-I superconductors. *Phys. Rev. B* **72**, 212508 (2005).

41. Prozorov, R. Equilibrium Topology of the Intermediate State in Type-I Superconductors of Different Shapes. *Phys. Rev. Lett.* **98**, 257001 (2007).

42. Jeudy, V., Gourdon, C. & Okada, T. Impeded growth of magnetic flux bubbles in the intermediate state pattern of type I superconductors. *Phys. Rev. Lett.* **92**, 147001 (2004).

43. Schawlow, A. L. & Devlin, G. E. Intermediate state of superconductors: Influence of crystal structure. *Phys. Rev.* **110**, 1011–1016 (1958).

44. Huebener, R. P. & Kampwirth, R. T. Intermediate state structure in superconducting films of Indium. *Phys.*

Status Solidi **13**, 255–263 (1972).

45. Fortini, A. & Paumier, E. Thermodynamics of metastable processes in the magnetization of type-I superconductors. *Phys. Rev. B* **14**, 55–60 (1976).

46. Prozorov, R. & Kogan, V. G. Effective Demagnetizing Factors of Diamagnetic Samples of Various Shapes. *Phys. Rev. Appl.* **10**, 014030 (2018).

47. Atzori, M. *et al.* Room-Temperature Quantum Coherence and Rabi Oscillations in Vanadyl Phthalocyanine: Toward Multifunctional Molecular Spin Qubits. *J. Am. Chem. Soc.* **138**, 2154–2157 (2016).

48. Camargo, L. C. *et al.* Exploring the Organometallic Route to Molecular Spin Qubits: The [CpTi(cot)] Case. *Angew. Chemie* **133**, 2620–2625 (2021).

49. Végh, J. The analytical form of the Shirley-type background. *J. Electron Spectros. Relat. Phenomena* **46**, 411–417 (1988).

50. Ohresser, P. *et al.* DEIMOS: A beamline dedicated to dichroism measurements in the 350–2500 eV energy range. *Rev. Sci. Instrum.* **85**, 013106 (2014).

51. Nakajima, R., Stöhr, J. & Idzerda, Y. U. Electron-yield saturation effects in $\boldsymbol{L}$ -edge x-ray magnetic circular dichroism spectra of Fe, Co, and Ni. *Phys. Rev. B* **59**, 6421–6429 (1999).

52. Brouder, C. Angular dependence of X-ray absorption spectra. *J. Phys. Condens. Matter* **2**, 701–738 (1990).

53. Cucinotta, G. pyDichroX. Available at: https://github.com/BeppeC/pyDichroX.

Supplementary Files

This is a list of supplementary files associated with this preprint. Click to download.

- SerranoSupplementaryInformation.docx